Received: 25 April 2022 | Revised: 13 June 2022 | Accepted: 31 July 2022

DOI: 10.1111/ijac.14158

International Journal of Applied Ceramic Technology

SPECIAL ISSUE ARTICLE

Low-temperature thermal energy storage with polymer-derived ceramic aerogels

Andrea Zambotti[1] | **Mattia Biesuz**[1] | **Mauro Bortolotti**[1] | **Andrea Dorigato**[1,2] | **Francesco Valentini**[1,2] | **Giulia Fredi**[1,2] | **Gian Domenico Sorarù**[1]

[1]Department of Industrial Engineering, University of Trento, Trento, Italy

[2]National Interuniversity Consortium of Materials Science and Technology (INSTM), Firenze, Italy

Correspondence
Andrea Zambotti, Department of Industrial Engineering, University of Trento, Via Sommarive 9, 38123 Trento, Italy.
Email: andrea.zambotti-1@unitn.it

Funding information
Andrea Zambotti, Mattia Biesuz, and Gian Domenico Sorarù acknowledge the financial support of the Italian Ministry of University and Research (MIUR) within the Programs PRIN2017-2017PMR932 "Nanostructured Porous Ceramics for Environmental and Energy Applications."

Abstract

Thermal energy storage (TES) with phase change materials (PCMs) presents some advantages when shape-stabilization is performed with ceramic aerogels. These low-density and ultra-porous materials guarantee high energy density and can be easily regenerated through simple pyrolysis while accounting for moderate mechanical properties. However, the small pore size that typically characterizes these sorbents can hinder the crystallization of PCMs, slightly reducing the energy density of the stabilized compound. In this work, we present the use of polymer-derived mesoporous SiC and SiOC aerogels for the stabilization of polyethylene glycol and a fatty alcohol (PureTemp 23), having a melting temperature of 17 and 23°C, respectively. Their TES performances point out maximum thermal efficiency values of around 80%. These performances are discussed accounting for the results of thermogravimetric analysis, differential scanning calorimetry, and leaking tests.

KEYWORDS
aerogel, phase change material, polymer derived ceramics, thermal energy storage

1 | INTRODUCTION

Efficiency in thermal energy management is nowadays becoming a relevant target for global warming mitigation. The substitution of conventional fossil-fueled power plants with green technologies that exploit renewable energy sources poses the problem of energy fluctuation that can be mitigated by developing proper storage technologies.[1] Accordingly, energy storage technologies have been largely improved, resulting in the development of new systems and materials in the fields of electrochemical, thermochemical, and thermal energy management.[2,3] Although the first two are characterized by energy release as chemical reactions occur, thus having the great advantage of allowing long-term energy storage, phase change materials (PCMs) are widely employed for thermal energy storage (TES), owing to their remarkable enthalpy of fusion. In this frame, TES is time-limited by heat losses that interest the molten PCM, thus offering a short-term energy storage (hours, days), depending on the designed solution.[4] PCMs for low-, medium-, and high-temperature applications have been extensively engineered to possess a high heat of fusion, as demonstrated by the use of eutectic salt mixtures for solar energy harvesting, or by the development of novel polymeric PCMs for low-temperature mitigation.[5] As a matter of fact, TES technologies are

easily customizable for the required application, ranging from heat recovery from industrial plants to renewable energy harvesting or temperature mitigation in buildings.[6–8]

Room temperature TES is one of the most promising solutions to reduce the energy consumption in buildings, as it gives the possibility to damp temperature fluctuations during daytime and nighttime. Such potential has attracted the scientific community,[9–13] as it represents a solid pathway to match the European Union target of boosting the construction of nearly zero-energy buildings.[14] Among available PCMs having a solid–liquid phase change at room temperature (say in the 10–40°C range), organic ones represent the great majority. Typical examples are given by polyethylene glycol, paraffine wax, and fatty acids, which can be incorporated within building components, thus offering a passive temperature damping effect, or used as a direct source of heat when implemented in air-conditioning systems.[15–17] However, problems related to the environmental sustainability and the end-of-life of organic PCMs must be considered before any direct application, and in this frame, bioderived, nontoxic PCMs are the most intriguing ones.

The containment of molten PCMs within porous matrices, thanks to capillary forces, is fundamental to guarantee a shape-stabilization and to avoid PCMs losses while optimizing the thermal efficiency of confined compounds. With respect to metallic and organic scaffolds, porous ceramics offer chemical inertness, relatively low density and high-temperature stability, thus being also attractive for the containment of corrosive salts.[18–21] In particular, polymer-derived ceramics (PDCs) are of great interest in this field, as properties like surface area and total porosity of the final products can be easily controlled during the synthesis route,[22–25] thus giving the possibility to obtain extremely porous ceramics, such as silicon-based aerogels.[26–28] As a matter of fact, PDCs are obtained through the controlled pyrolysis of polymeric precursors, which can be chemically engineered to obtain exotic compositions (e.g., SiBCN, SiAlON, and SiCN) with unprecedented functionalities.[29,30]

This article reports the synthesis and the use of polymer-derived silicon carbide (SiC) and silicon oxycarbide (SiOC) aerogels as shape-stabilizers for organic room temperature PCMs. The rationale behind the use of this type of skeleton materials lies on three milestones: (i) both SiC and SiOC aerogels display high pore volume and specific surface area (SSA) and can be synthesized to have over-stoichiometric carbon (i.e., free carbon) in their structure in order to boost the thermal conductivity of the ceramic network (in a previous study, we showed how free carbon can mitigate the rather low thermal conductivity of SiOC when dealing with thermochemical heat storage[31]); (ii) PDCs aerogels possess a mechanically stable hierarchical porosity[32] in the mesopore–macropore range able to minimize molten PCM losses; (iii) both SiC and SiOC are nontoxic safe silicon-based ceramics.

Finally, with the aim of processing an ecological sustainable material, we selected two biopolymers, that is, polyethylene glycol and PureTemp 23 (a 1-dodecanol-based bioderived compound), as PCMs for low-temperature TES, to be shape-stabilized by the novel ceramic aerogels. The paper reports the details of the synthesis together with the chemical and microstructural characterization of the PDC aerogels. The thermal properties of the stabilized PCMs have been characterized by differential scanning calorimetry (DSC), and the results have been discussed and related to the features (porosity, pore size, and chemistry) of the porous ceramic aerogel.

2 | EXPERIMENTAL PROCEDURES

2.1 | Synthesis procedure

StarPCS SMP-10 polycarbosilane and Polyramic SPR-036 polysiloxane (Starfire Systems Inc., NY, USA) were utilized as precursors for the synthesis of aerogels belonging to the SiC and SiOC systems, respectively.

SMP-10 was cross-linked with divinylbenzene via hydrosilylation reaction (DVB, Sigma-Aldrich, CAS: 1321-74-0) imposing a 1:1 molar ratio between Si–H and vinyl groups of DVB, using cyclohexane as a solvent (Carlo Erba, Milano, Italy). To favor hydrosilylation, 100 μl of Karstedt's catalysts (Sigma-Aldrich, Saint Louis, MO, USA, CAS: 68478-92-2), diluted to .1% Pt in xylene, were added per gram of resin. Similarly, preceramic SiOC aerogels were synthesized by mixing in *n*-hexane (PanReac, CAS: 110-54-3) SPR-036 and DVB in a 1:1 weight ratio and adding 50 μl of diluted catalyst per gram of polymer. In both syntheses, the solvent volume fraction was set to 90% of the total solution. Gelation was performed at mild temperatures within a digestion vessel (Model 4749, Parr Instrument Company, Moline, IL, USA) to prevent any solvent evaporation. Polycarbosilane gels formed after 5 h at 150°C, whereas polysiloxane ones required a 24-h dwell at 180°C. As typically done,[33] the obtained gels were subjected to a two-step solvent exchange: (i) washing in a fresh solvent six times (twice per day) to remove unreacted species; (ii) exchange of an organic solvent with liquid CO_2 by means of six washing cycles (twice per day) in a customized autoclave. CO_2 supercritical drying was finally carried out to obtain the preceramic samples. The ceramization of SiOC and SiC/C aerogels was achieved pyrolyzing the samples at 800°C (1-h dwell at 800°C, 5°C min^{-1}, 300 cm^3 min^{-1} N_2).

TABLE 1 Labeling system adopted for the aerogel-stabilized phase change materials (PCMs)

Type of resin	Pyrolysis temperature (°C)	PCM	Impregnation methodology	Label
SMP-10	800	PEG	Environment	SiC/C-800-PEG (E)
			Vacuum	SiC/C-800-PEG (V)
		PureTemp 23	Environment	SiC/C-800-PT (E)
			Vacuum	SiC/C-800-PT (V)
SPR-036	800	PEG	Environment	SiOC-800-PEG (E)
			Vacuum	SiOC-800-PEG (V)
		PureTemp 23	Environment	SiOC-800-PT (E)
			Vacuum	SiOC-800-PT (V)

Aerogel-stabilized polyethylene glycol 600, PEG, (Alfa Aesar, Thermo Fisher GmbH Kandel, Germany) and PureTemp 23, PT, (Octochem Inc., Vandalia, USA) were produced by ambient pressure impregnation and vacuum impregnation. In both cases, impregnation was carried out in an autoclave kept at 40°C by soaking the aerogel matrices into the molten PCMs for 30 min. Vacuum was eventually applied for the impregnation of the homonymous series of specimens. The two impregnation procedures were considered completed when no bubbles nucleated any longer on the aerogels surface, suggesting that the available porosity was completely filled with the molten PCMs.

According to the available physical properties on the technical datasheet, polyethylene glycol presents a melting temperature in the range of 17–23°C, a density of 1.12 g cm^{-3}, and a molecular weight of 600 g mol^{-1}. Similarly, PureTemp 23 melts at 23°C with an enthalpy of fusion of 227 J g^{-1}, and a density of .83 g cm^{-3}. Table 1 provides the labeling system adopted for the samples described in this paper.

2.2 | Characterization methodologies

The morphology of the ceramic aerogels were investigated by a scanning electron microscope (SEM) using a Gemini SUPRA 40 FE-SEM (Carl Zeiss, Germany) facility. To account for the SSA and the pore size distribution, N_2 adsorption and desorption isotherms were acquired with an ASAP 2020 apparatus (Micromeritics, Norcross, GA, USA) at 77 K. The isotherms were processed following the Brunauer–Emmett–Teller theory and the Barrett–Joyner–Halenda method for the calculation of pores size distribution.[34]

Skeletal densities of ceramic aerogels were assessed with an AccuPyc 1330 pycnometer (Micromeritics, Norcross, GA, USA) at 23°C.

Infrared spectra of neat and stabilized PCMs were acquired in transmission mode with a Nicolet Avatar 330 FT-IR spectrophotometer (Thermo Fischer Scientific, Waltham, MA, USA), using KBr pellets and collecting 64 scans with an imposed resolution of 4 cm^{-1}.

X-ray diffraction (XRD) patterns of the crystallized PCMs confined within the aerogel scaffolds were acquired with an Italstructures IPD3000 diffractometer equipped with Cu anode X-Ray source coupled to a multilayered monochromator and a 1024-channel Dectris Mythen linear strip detector. Data acquisition was carried out over the 10°–100° 2θ range with a total acquisition time of 30 min per sample. All specimens were placed in a customized sample holder with direct contact to a liquid nitrogen bath to avoid melting phenomena relative to the PCMs exposure to the room temperature (ca. 20°C) during the acquisition time.

The capability of the impregnated samples to retain paraffin was investigated through a leaking test performed in an oven at 40°C. The specimens were placed on an absorbent paper towel, and their mass was monitored for 8 days to determine the maximum quantity of PCM that they were able to retain. The residual PCM content was calculated as a fraction of weight with respect to the weight of each sample without PCM.

Thermogravimetric analysis (TGA) of neat and stabilized PCMs was performed with a TA-I Q5000 IR under a nitrogen flow of 10 cm^3 min^{-1} in a temperature interval between 30 and 700°C, at a heating rate of 10°C min^{-1}. The temperature associated with a mass loss of 5% ($T_{5\%}$), and the temperature associated with the maximum degradation rate (T_{peak}) were determined. In order to determine the effective PCM content, the residual mass after PCM degradation (m_{degPCM}) was evaluated: It corresponds to the residual mass at 200°C for PT-impregnated samples and to the residual mass at 500°C for impregnated samples.

Differential scanning calorimetry (DSC) of neat and stabilized PCMs was performed with a Mettler DSC30

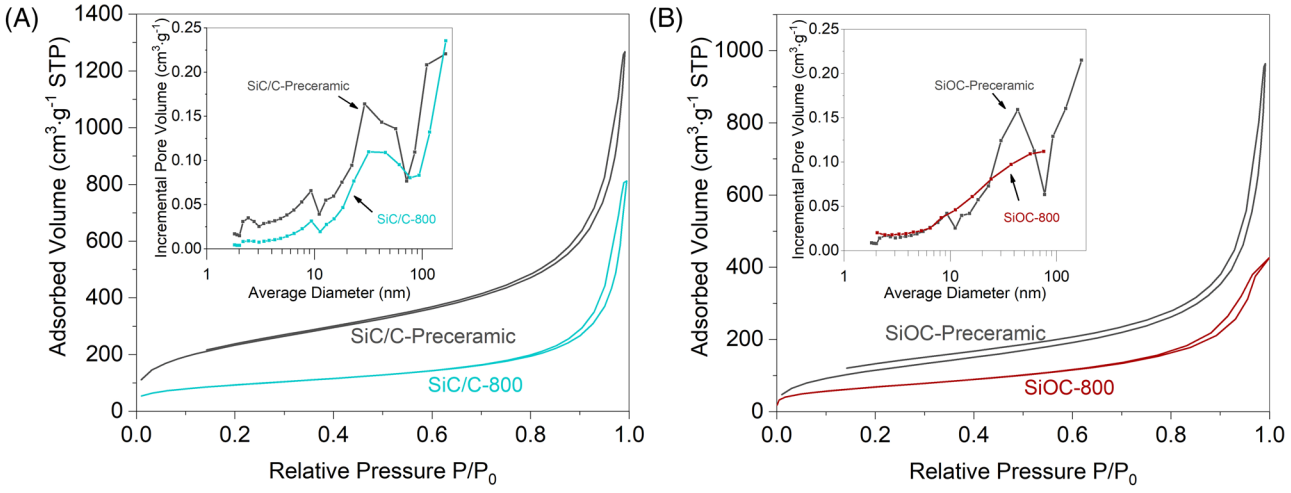

FIGURE 1 Nitrogen adsorption/desorption isotherms and calculated pores size distributions (insets) of: (A) SiC/C aerogel before and after pyrolysis; (B) SiOC aerogel before and after pyrolysis

calorimeter (Mettler Toledo, Inc., Columbus, OH, USA). Samples of neat PCMs and PCM-impregnated aerogels of ~5 mg were subjected to a heating–cooling–heating cycle at 1°C min^{-1}, under an N_2 flow of 100 ml min^{-1}. The investigated temperature interval was −30/30°C for the samples containing PEG and −5/30°C for the samples containing PureTemp 23. One specimen was tested for each sample. This test allowed the measurement of the melting and crystallization temperatures (T_m, T_c) and specific melting/crystallization enthalpy values (ΔH_m, ΔH_c). An estimation of the crystallized PCM weight fraction in the aerogels was calculated by dividing the phase change enthalpy of the impregnated aerogel by that of the neat PCM. By comparing this result with that of TGA and leaking tests, it was possible to assess whether a certain fraction of PCM did not crystallize due to the confinement in the aerogels mesopores.

3 | RESULTS AND DISCUSSION

3.1 | Characterization of neat aerogels

The SSA and the pore size distribution of the ceramic aerogels were measured by recording N_2 physisorption isotherms (Figure 1). The isotherm shapes give information about the type of a sorbent analyte. In particular, the IUPAC classification defines the presented curves as Type IV isotherms, typical of mesoporous sorbents (pore diameter in 2–50 nm range[35]). Even though SiOC and SiC/C curves might seem to have a Type II characteristic, which is relative to macroporous sorbents, an inflection point near the saturation pressure ($P/P_0 \sim 1$, especially visible in SiOC-800) identifies the mesoporous characteristic.

TABLE 2 Summary of nitrogen physisorption resulting specific surface areas (SSAs) and pore volumes, and skeletal densities of ceramic aerogels obtained through He pycnometry

	SSA ($m^2\ g^{-1}$)	V_p ($cm^3\ g^{-1}$)	ρ_s ($g\ cm^{-3}$)
SiC/C preceramic	837	1.87	–
SiOC preceramic	427	1.47	–
SiC/C-800	325	1.21	1.82 ± .01
SiOC-800	248	.67	1.77 ± .01

More properly, these aerogels can be defined as hierarchically porous sorbents, as suggested by SEM micrographs in Figure 2, where pores with diameters of hundreds of nanometers are visible. Such conclusion can be outlined from the H1-type hysteresis loops between adsorption and desorption branches at high P/P_0, which are not completely vertical, meaning that the capillary condensation of N_2 occurs over pores with a wide size distribution.[36] As a matter of fact, the insets in Figure 1A,B show that in all aerogels, the pore volume increases starting from 2 nm to reach the detectable maximum over 100 nm. Table 2 summarizes N_2 physisorption results and shows that SiC/C-800 aerogels possess higher SSA and mesopore volume with respect to SiOC ones. Finally, both kinds of ceramic aerogels are characterized by a colloidal morphology, where primary colloidal particles seem smaller in SiOC-800 with respect to those of SiC/C-800.

Despite the compositional difference between the two ceramics, skeletal densities (Table 2) fall in the 1.77–1.82 g cm^{-3} range. Such values result smaller than those of silicon carbide (3.21 g cm^{-3}, in Ref. [37]), silicon oxycarbide (2.22 g cm^{-3} at 1100°C, in Ref. [38]), and even sp^2 graphitic carbon (2.27 g cm^{-3}, in Ref. [39]), underlying that at the nanoscale, these aerogels present a high free volume

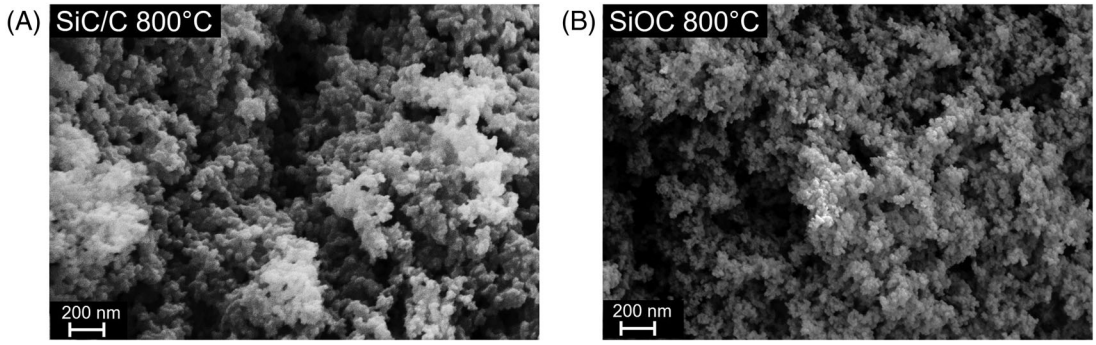

FIGURE 2 Field-emission scanning electron microscope (FE-SEM) micrographs of ceramic aerogels: (A) SiC/C-800; (B) SiOC-800

FIGURE 3 FT-IR spectra of neat and stabilized phase change materials (PCMs) (vacuum impregnated samples)

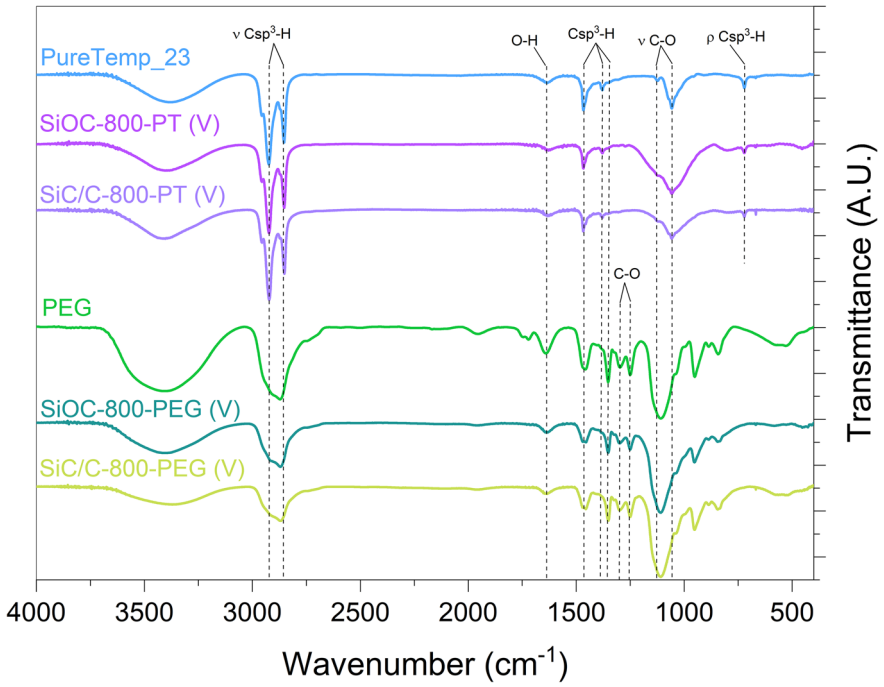

of the amorphous structure, which at 800°C is still preserved. Similar results have been reported for SiOC glasses with significant fractions of free carbon.[40]

3.2 | Impregnation with PCMs

After impregnation, stabilized PCMs were characterized by means of FT-IR spectroscopy to detect any possible interaction between ceramic aerogels and heat storage media. In particular, we report the spectra relative to vacuum impregnated specimens. The rationale behind this selection lies in the fact that we expect the smallest aerogels pores to be impregnated more easily in vacuum rather than in ambient conditions, and interfacial interactions preferably occur in cavities provided with high surface-to-volume ratio. Acquired infrared spectra are reported in Figure 3. As can be easily observed, composite specimens present the same vibrational peaks of the neat PCMs without any signal of additional bonds. Only SiOC-800-PT shows a wide signal centered at 1100 cm^{-1}, which can be attributed to Si–O bond vibrations of the ceramic skeleton. PureTemp 23 presents absorbance signals of –OH groups at 3320 cm^{-1}, and H-Csp^3 at 2960, 2920, and 2857 cm^{-1}, respectively. At lower wavenumbers, namely, at 1464 and 1377 cm^{-1}, C–H bending signals can be observed. Peaks at 1128 and 1056 cm^{-1} can be attributed to C–O stretching vibrations in secondary and primary alcohols, respectively. The weak signal at 720 cm^{-1} is relative to the out-of-plane rocking of C–H bonds. As we already reported,[41] PureTemp 23 seems to be composed of a blend of alcohols, where 1-dodecanol has a predominant fraction.[42] Similarly, polyethylene glycol presents a broad O–H signal centered at 3400 cm^{-1}, sp^3-hybridized carbon signals in the 2980–2815 and 1500–750 cm^{-1} ranges. C–OH bond stretching can be found at 1297, 1250, and 1190 cm^{-1},

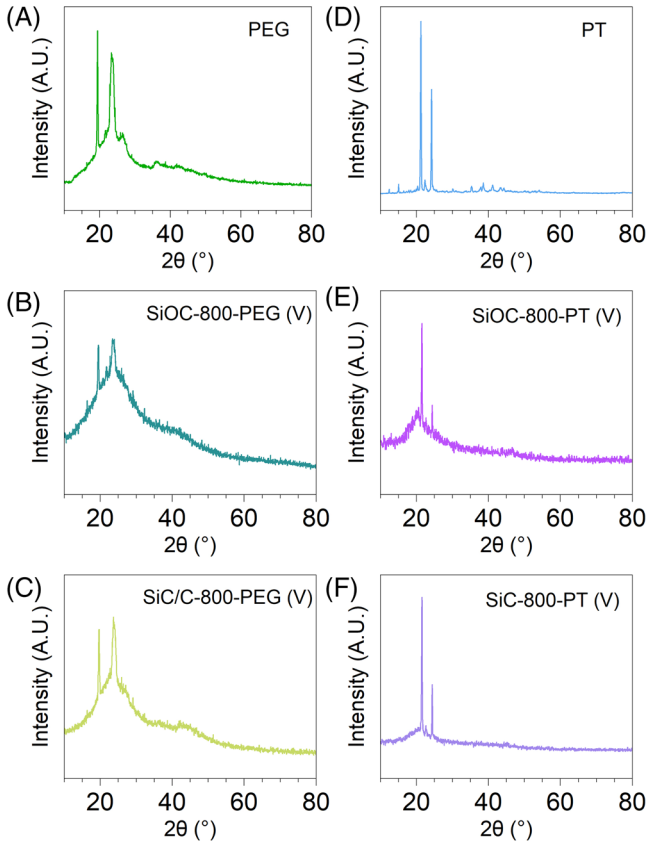

FIGURE 4 X-ray diffraction (XRD) patterns of neat (A, D) and stabilized (B, C, E, F) phase change materials (PCMs) (vacuum-impregnated samples)

whereas the peaks at lower wavenumbers are attributed to C–C and C–O bonds.[43] As Si–O–Si (1090 cm^{-1}) and Si–C (770 cm^{-1}) bond contributions to the overall absorption of the infrared beam are negligible with respect to those of PCMs, we do not report any assignment to ceramic bonds.[44] In conclusion, no chemical interaction with the aerogels can be alleged from these spectra.

XRD patterns of vacuum impregnated aerogels were acquired to look for any crystallographic difference between neat and confined crystallized PCMs. As a matter of fact, it is known that the confinement of polymers in small pores might favor the crystallization of metastable phases at room temperature.[45] From a thermodynamical point of view, this typically affects the thermal performances of the PCM, owing to the fact that the enthalpy of fusion is reduced.

Figure 4 reports powder diffraction data collected on stabilized PEG and PureTemp 23 when vacuum impregnation is used.

The XRD pattern collected on neat PEG (i) shows the typical features of a semicrystalline compound, with two sharp Bragg peaks at 19.5° and 23.5° as well as a diffuse signal with two broad maxima located at about 23° and 40°, arising from the amorphous fraction of the material. Data collected on the two impregnated aerogels (ii) and (iii) clearly show still the presence of the two characteristic PEG diffraction peaks, whereas the diffuse part of the pattern also accounts for the scattering of the amorphous aerogels, with another broad peak shoulder that is located at about 20° for both compounds. In the absence of a crystallographic model, no sophisticated microstructural modeling can be performed (e.g., by means of the Rietveld method); however, assuming an isotropic crystallite shape and the absence of lattice strain, an approximate crystallite size estimation can be obtained applying the semiempirical Williamson–Hall method. In this case, an average volume-weighted crystallite size of 59, 31, and 28 nm is obtained for neat PEG, PEG–SiC, and PEG–SiOC composites, respectively, suggesting a loss of crystalline ordering when the PCM crystallizes in the aerogels matrix.

A similar behavior is observed with the PureTemp 23 composites. The pattern collected on pure crystalline 1-dodecanol (iv) exhibits two main diffraction peaks at $2\theta = 25°$ and 28.4°, along with secondary reflections located at 12.4°, 15.0°, and in the 30°−45° region. Again, the patterns of the two composites (v) and (vi) show still the presence of the two major PT Bragg reflections, along with the diffuse signal arising from the amorphous aerogels; additional minor Bragg reflections from PT are clearly missing, probably due to the loss of long-range (low angle peaks) and short-range (high angle peaks) crystalline ordering. Average crystallite sizes calculated for PureTemp 23 are 82, 42, and 62 nm for neat PT, PT–SiC, and PT–SiOC respectively, additionally pointing to a decrease in crystallinity for confined crystallized PCMs. To conclude, it can be reasonably assumed that in both cases, no significant modification from the crystallographic point of view (e.g., due to polymorph crystallization) takes place, and only microstructural changes are in effect.

Leaking tests were performed to evaluate which combination of PCM type (PEG or PT), aerogel type (SiC/C or SiOC), and impregnation method (vacuum or environmental) yielded a higher retained PCM mass fraction. The results are shown in Figure 5A,B. From the curves obtained for vacuum-impregnated samples (Figure 5A), it is evident that the PCM leakage is very limited for both PEG and PT and occurs mainly in the first day, probably due to the loss of excess PCM from the sample surface. The aerogel type that is able to absorb the highest quantity of both PCMs is SiC/C, for which the final PCM weight fractions are 84.4 wt% for PEG and 75.1 wt% for PT. For both aerogels, PEG seems to be the one with the higher affinity and therefore absorbed in higher amounts.

The impregnation under environmental conditions (Figure 5B) leads to similar results of vacuum impregnation in the case of PEG and PT. In particular, the

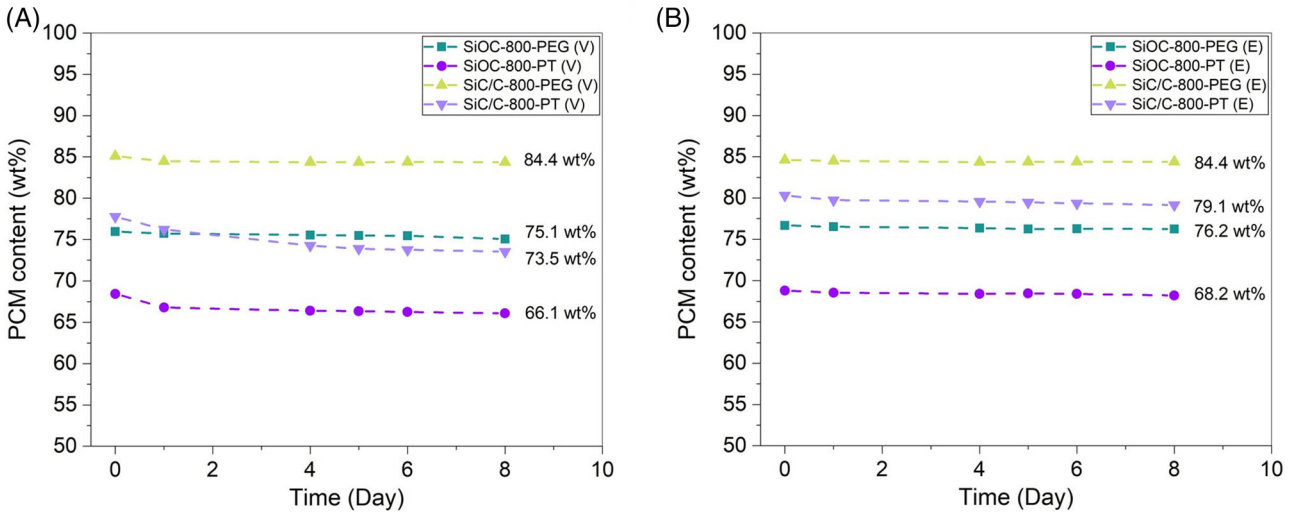

FIGURE 5 Results of the leaking tests at 40°C: (A) vacuum-impregnated samples; (B) environment-impregnated samples

SiC/C-800-PT (E) sample has a residual PCM content at the end of the test equal to 79.1 wt%, whereas the SiC/C-800-PT (V) has a content of 73.1 wt%. It can also be observed that the PCM loss in the case of environmental impregnation seems more limited with respect to vacuum impregnation. Also in this case, it can be verified that the SiC/C matrix absorbs higher amounts of PCM compared to SiOC and that PEG is absorbed in larger quantities with respect to PT. Possibly, such differences arise from two aspects: First, SiC/C aerogels possess a higher porosity, thus being able to retain higher fractions of PCMs with respect to SiOC. Second, it is clear that PEG penetrates more easily than PT in the aerogels matrices, thus suggesting that it has a lower surface tension at the impregnation temperature of 40°C. Unfortunately, no data on these physical properties of PureTemp 23 are available to support this assumption.

TGA was performed to understand the thermal degradation resistance of the impregnated samples, to verify the effect of the matrix on the degradation of the absorbed PCM, and to determine the effective PCM content in each sample. The residual mass and derivative curves of environment-impregnated samples are shown in Figure 6A,B, whereas the most important results are listed in Table 3. The curves of vacuum-impregnated samples are not shown for the sake of brevity.

The degradation of neat PEG (Figure 6A) occurs in a singles step: It starts at ~316°C ($T_{5\%}$) and reaches the maximum speed at 408°C (T_{peak}). Impregnated samples containing PEG show an initial limited weight loss in the temperature range 100–200°C, which leads to a progressive decrease of their $T_{5\%}$ values. This behavior may be related to absorbed moisture, but further analysis is needed to clarify this point. After this limited initial weight loss, impregnated samples show the degradation of PEG occurring at ~360–370°C, as it is possible to observe from the derivative curves shown in Figure 6B. Compared to neat PEG, the degradation observed in the impregnated samples starts at lower temperatures and covers a broad temperature range. This behavior may be related to the surface contact with the aerogel walls, the presence of which is expected to increase the solid thermal conductivity of the composite compared to that of the neat PCM. For the PT-containing samples, the degradation of neat PT occurs very rapidly in a single step, starting at approximately 120°C ($T_{5\%}$) and reaching the maximum speed at 178°C (T_{peak}). Differently from PEG-containing samples, PT-impregnated samples show very similar degradation curves as neat PT, with comparable values of $T_{5\%}$ and T_{peak}. Such difference between the two stabilized PCMs

TABLE 3 Results of thermogravimetric analysis (TGA) tests on neat phase change materials (PCMs) and on the impregnated samples

Sample	$T_{5\%}$ (°C)	T_{peak} (°C)	m_{degPCM} (wt%)
PEG	316	408	1.6
SiC/C-800-PEG (E)	218	366	19.5
SiC/C-800-PEG (V)	126	368	20.5
SiOC-800-PEG (E)	248	374	26.5
SiOC-800-PEG (V)	253	360	28.9
PureTemp_23	120	179	0.0
SiC/C-800-PT (E)	105	147	26.5
SiC/C-800-PT (V)	115	164	28.8
SiOC-800-PT (E)	123	159	36.5
SiOC-800-PT (V)	112	153	35.2

Note: $T_{5\%}$ is the temperature corresponding to a weight loss of 5 wt%; T_{peak} is the temperature corresponding to the peak of the derivative curve); m_{degPCM} is the residual mass after degradation of PT (200°C) and PEG (500°C), respectively.

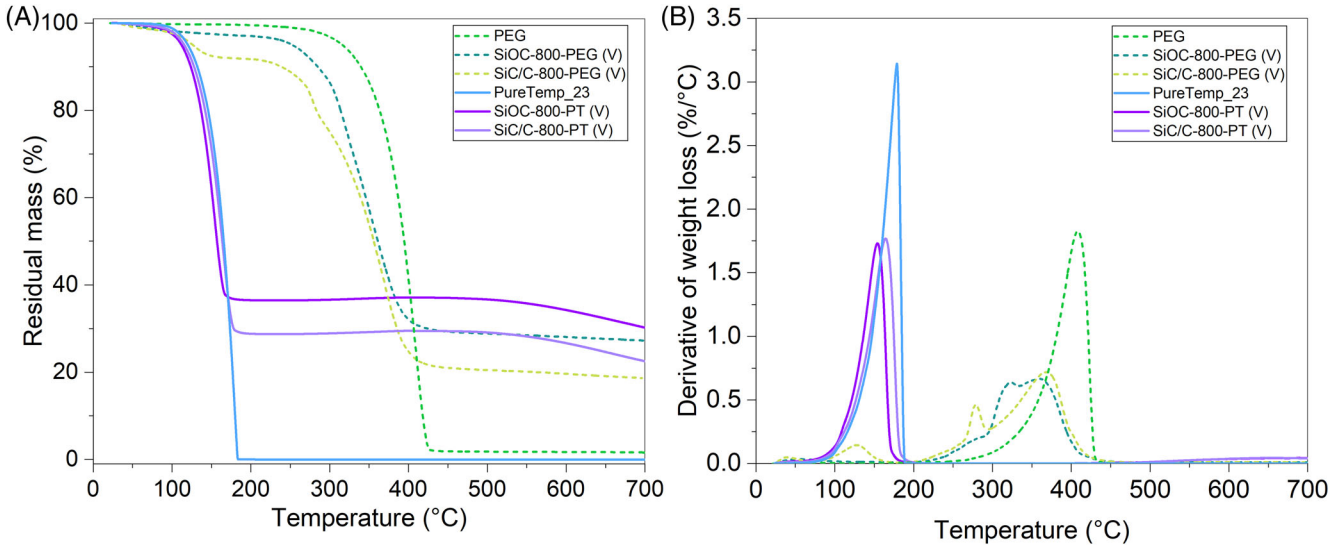

FIGURE 6 Residual mass curves from N_2 thermogravimetric analysis (TGA) tests: (A) neat phase change materials (PCMs) and samples impregnated under atmospheric pressure; (B) derivatives curves of the TGA curves reported in (A)

should be clarified as it suggests that the thermal stability of PEG is somehow affected by the presence of the ceramic component.

Focusing on the aerogel type, it can be observed that the use of SiOC or SiC/C aerogels does not substantially influence the thermal degradation behavior of the samples. On the other hand, the higher degradation temperature of PEG-impregnated samples may allow the use of these samples for particular applications where the use of other PCMs, like PT or paraffin, is not possible due to their lower temperature resistance.[46] The residual mass values at 200 and 500°C allow the evaluation of the effective PCM content of PT- and PEG-impregnated samples, respectively.

DSC tests were performed to measure the TES performance of the prepared composites and to highlight any difference between the two PCMs and the two aerogels in terms of the extent and the temperature interval of latent heat storage. Figure 7 shows the DSC thermograms of the neat PCMs and the impregnated aerogels, whereas Table 4 collects the main DSC results, that is, the phase change temperatures and enthalpy values.

Neat PEG presents an endothermic melting peak between 0 and 15°C and a corresponding exothermic peak between 10 and −5°C, associated with a latent heat of approximately 140 J g^{-1}. Similarly, neat PureTemp 23 shows an endothermic melting peak between 15 and 25°C and a corresponding exothermic peak between 15 and 5°C, with a latent heat of ~218 J g^{-1}. The same transitions can be also observed in all the PCM-impregnated aerogels. Here, the melting phenomenon is slightly anticipated and the crystallization phenomenon slightly delayed compared to neat PCMs, as observable from the small but

TABLE 4 Main results of the DSC tests (second heating scan and cooling scan) on neat phase change materials (PCMs) and impregnated aerogels

Sample	T_m (°C)	ΔH_m (J g^{-1})	T_c (°C)	ΔH_c (J g^{-1})
PEG	16.9	141.0	6.8	134.5
SiC/C-800-PEG (E)	14.6	110.8	7.7	102.4
SiC/C-800-PEG (V)	14.1	113.8	7.3	107.5
SiOC-800-PEG (E)	14.4	85.5	7.6	76.0
SiOC-800-PEG (V)	14.2	76.8	5.7	76.3
PureTemp_23	22.2	217.6	14.1	218.4
SiC/C-800-PT (E)	20.7	141.7	10.6	137.2
SiC/C-800-PT (V)	20.2	141.5	9.6	134.5
SiOC-800-PT (E)	19.9	119.6	10.1	115.0
SiOC-800-PT (V)	19.7	124.7	9.6	115.3

Note: T_m, ΔH_m is the melting temperature and enthalpy, second heating scan; T_c, ΔH_c is the crystallization temperature and enthalpy.

significant differences in the phase change peak temperatures (Table 4), and especially in the cooling scan of the PureTemp 23-containing aerogels (Figure 7D). This suggests that the nucleation of PCM crystals from the melt is hindered by the confinement in the small aerogel pores, so that smaller crystallites are formed, thus favoring the subsequent melting phenomenon due to the larger fraction of grain boundaries. This finding, supported by the XRD results, has been reported for other PCMs confined in mesopores.[45,47] However, the operating temperature ranges in which the composites can effectively store and release heat are not significantly different from those of the neat PCMs. Moreover, the impregnation method (E or

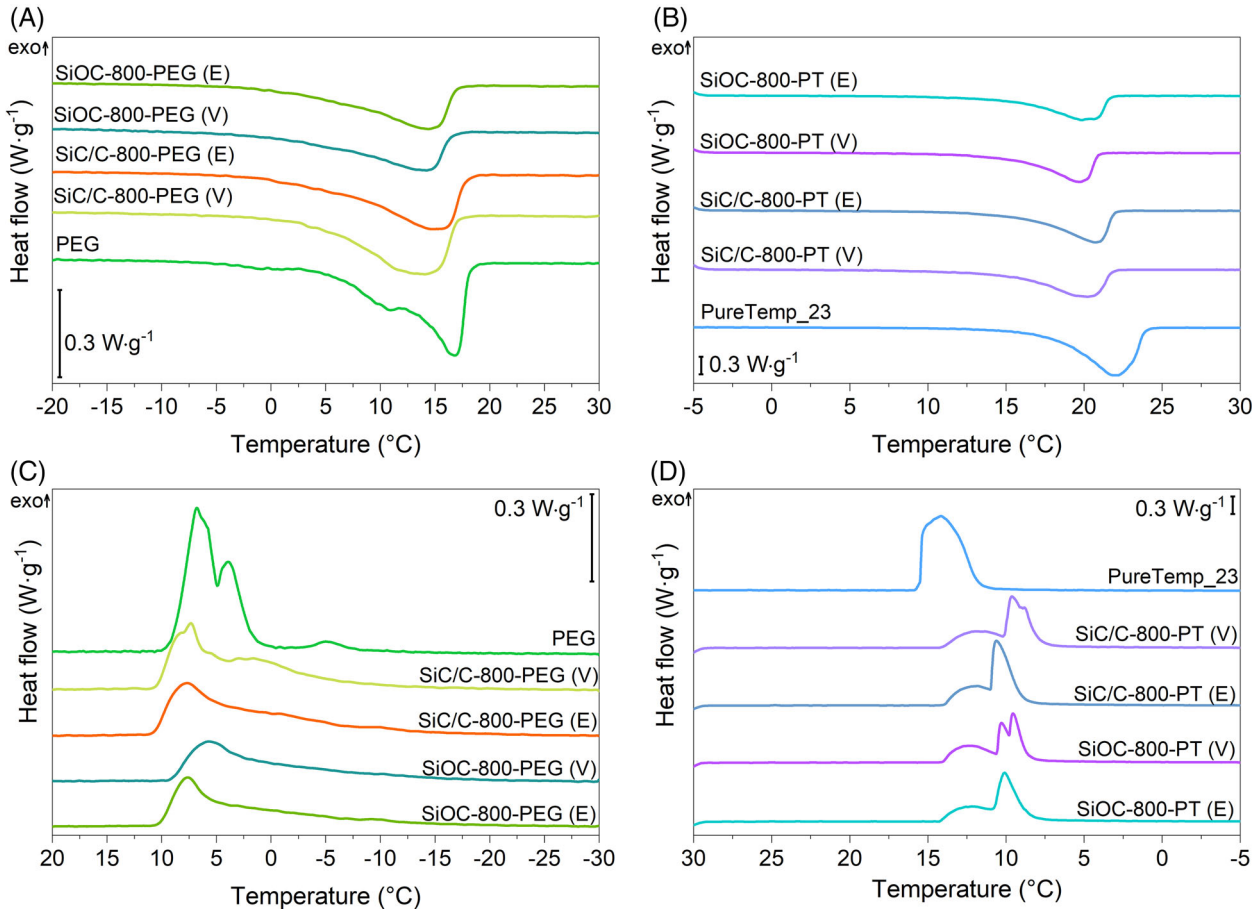

FIGURE 7 DSC thermograms of neat phase change materials (PCMs) and impregnated aerogels (A and B) second heating scan; (C and D) cooling scan

V) and the aerogel type do not affect this phenomenon substantially.

For the latent heat values that express the TES performance of the samples, the larger phase change enthalpy of PureTemp 23 compared to PEG accounts for the higher TES performance of the PureTemp 23-containing composites. Moreover, the composites based on SiC/C aerogels always show a higher phase change enthalpy compared to those based on SiOC, because the larger SSA and pore volume (Table 2) allow for the accommodation of a larger PCM fraction, regardless of the PCM type.

These findings are in good agreement with the results of TGA and leaking test, through which a weight fraction of PCM was determined. The results of this evaluation are reported in Figure 8, which shows the PCM content (wt%) evaluated in three ways, that is, by the simple mass difference after the leaking test, by the mass loss in TGA due to PCM degradation, and the normalization of the phase change enthalpy of the composites by that of the neat PCMs measured in DSC. If the data from the leaking test and TGA agree with each other, the PCM content measured through DSC is generally underestimated. This phenomenon, especially evident for SiOC-based composites and for the PT-containing aerogels, implies that the crystallization of the PCMs is hindered by the confinement in small pore volumes of the surrounding aerogel, which results in a lower phase change enthalpy. This is in good agreement with the findings on the phase change temperatures. It is possible to hypothesize that this behavior is related to interactions between the PCM and the aerogel. In a previous work, the PCM content of aerogel samples impregnated with paraffin was almost identical if measured with DSC and leaking tests.[48] Similarly to this work, authors observed that pomelo peel samples impregnated with PT were characterized by lower PCM content if measured with DSC with respect to leaking tests.[41] Nevertheless, the heat storage/release capacity reached with these composites is quite interesting for TES applications. The highest TES performance is reached in the sample SiC/C-800-PT, exhibiting a melting enthalpy that reaches 141 J g^{-1}, comparable with that reached in a previous work with the same PCM embedded in porous biogenic structures.[41]

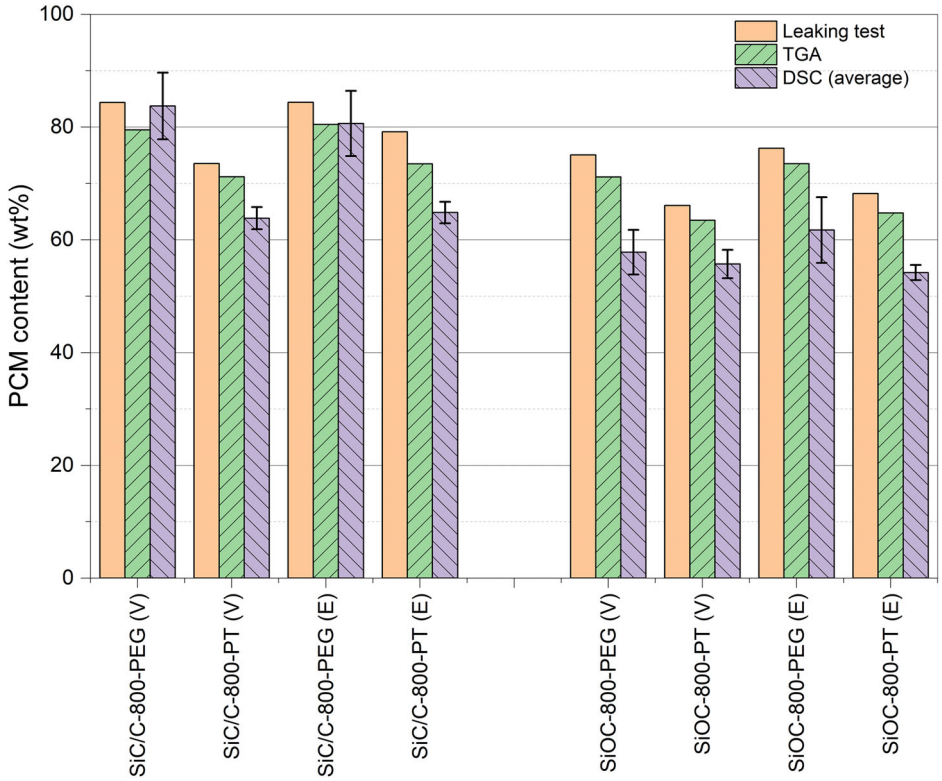

FIGURE 8 Phase change material (PCM) content (wt%) for the prepared samples evaluated through leaking test, thermogravimetric analysis (TGA), and DSC (average of three scans)

4 | CONCLUSIONS

Polymer-derived SiC and SiOC ceramic aerogels were synthesized and impregnated with two biopolymers, namely, polyethylene glycol and PureTemp 23 under vacuum and ambient pressure conditions. The thermal performances of the shape-stabilized PCMs were estimated via leaking tests, thermogravimetry, and DSC measurements. The outcomes of such analyses provide an insight in the optimal retaining capabilities of mesoporous aerogels, even when the weight fraction of the organic PCMs exceeds 84 wt%. Although no chemical interaction between the skeleton materials and the PCMs was clearly revealed, XRD and DSC results suggest that the crystallization behavior of the confined compounds is not optimal: Crystallites resulted smaller than those of neat PCMs and the melting/crystallization curves shifted to a lower temperature range, indicating early melting phenomena. In this frame, it is possible to consider SiC/C aerogels as the most promising ones for room temperature TES applications. As a matter of fact, a maximum enthalpy of fusion of 141.7 J g^{-1} was achieved with PureTemp 23, and a TES efficiency of 80.7% was reached by employing polyethylene glycol (calculated from DSC melting enthalpy ratio with neat PEG). Besides, ambient pressure impregnation was demonstrated to be competitive with vacuum impregnation, showing the manageability of these materials. In conclusion, this work provides preliminary results of successful use of ceramic aerogels to confine PCMs for room temperature TES.

ACKNOWLEDGMENT

Open Access Funding provided by Universita degli Studi di Trento within the CRUI-CARE Agreement.

ORCID

Andrea Zambotti https://orcid.org/0000-0002-8653-055X
Mattia Biesuz https://orcid.org/0000-0002-4338-4177
Mauro Bortolotti https://orcid.org/0000-0002-7213-6316
Andrea Dorigato https://orcid.org/0000-0002-4743-7192
Francesco Valentini https://orcid.org/0000-0001-9496-0501
Giulia Fredi https://orcid.org/0000-0001-9987-1786
Gian Domenico Sorarù https://orcid.org/0000-0002-0453-3379

REFERENCES

1. European Environment Agency. Regulation (EC) no 443/2009 of the European parliament and of the council of 23 April 2009

setting emission performance standards for new passenger cars as part of the community's integrated approach to reduce CO2 emissions from light-duty vehicles. Off J Eur Union. 2009;52:20.
2. Gür TM. Review of electrical energy storage technologies, materials and systems: challenges and prospects for large-scale grid storage. Energy Environ Sci. 2018;11(10):2696–767. https://doi.org/10.1039/c8ee01419a
3. Olabi AG, Onumaegbu C, Wilberforce T, Ramadan M, Abdelkareem MA, Al-Alami AH. Critical review of energy storage systems. Energy. 2021;214:118987. https://doi.org/10.1016/j.energy.2020.118987
4. Koohi-Fayegh S, Rosen MA. A review of energy storage types, applications and recent developments. J Energy Storage. 2020;27:101047. https://doi.org/10.1016/j.est.2019.101047
5. Pielichowska K, Pielichowski K. Phase change materials for thermal energy storage. Prog Mater Sci. 2014;65:67–123. https://doi.org/10.1016/j.pmatsci.2014.03.005
6. Royo P, Acevedo L, Ferreira VJ, García-Armingol T, López-Sabirón AM, Ferreira G. High-temperature PCM-based thermal energy storage for industrial furnaces installed in energy-intensive industries. Energy. 2019;173:1030–40. https://doi.org/10.1016/j.energy.2019.02.118
7. Stutz B, Le Pierrès N, Kuznik F, Johannes K, Del Barrio EP, Bedecarrats S, et al. Storage of thermal solar energy storage of thermal solar energy Stockage thermique de l'énergie solaire. C R Phys. 2017;18(8):401–14. https://doi.org/10.1016/j.crhy.2017.09.008
8. De Gracia A, Cabeza LF. Phase change materials and thermal energy storage for buildings. Energy Build. 2015;103:414–9. https://doi.org/10.1016/j.enbuild.2015.06.007
9. Fredi G, Dorigato A, Fambri L, Pegoretti A. Multifunctional epoxy/carbon fiber laminates for thermal energy storage and release. Compos Sci Technol. 2018;158:101–11. https://doi.org/10.1016/j.compscitech.2018.02.005
10. Dorigato A, Canclini P, Unterberger SH, Pegoretti A. Phase changing nanocomposites for low temperature thermal energy storage and release. Express Polym Lett. 2017;11(9):738–52. https://doi.org/10.3144/expresspolymlett.2017.71
11. Fredi G, Dorigato A, Pegoretti A. Multifunctional glass fiber/polyamide composites with thermal energy storage /release capability. Express Polym Lett 2018;12(4):349–64. https://doi.org/10.3144/expresspolymlett.2018.30
12. Dorigato A, Ciampolillo MV, Cataldi A, Bersani M, Pegoretti A. Polyethylene wax/EPDM blends as shape-stabilized phase change materials for thermal energy storage. Rubber Chem Technol. 2017;90:575–84. https://doi.org/10.5254/rct.82.83719
13. Fredi G, Dorigato A, Fambri L, Pegoretti A. Wax confinement with carbon nanotubes for phase changing epoxy blends. Polymers (Basel). 2017;9:405. https://doi.org/10.3390/polym9090405
14. European Union. Directive 2010/31/EU of the European Parliament and of the Council of 19 May 2010 on the energy performance of buildings. Off J Eur Union. 2010;153:16–35.
15. Valentini F, Morandini F, Bergamo M, Dorigato A. Development of eco-sustainable plasters with thermal energy storage capability. J Appl Phys. 2020;128(7):075103. https://doi.org/10.1063/5.0012139
16. Delgado M, Lázaro A, Mazo J, Zalba B. Review on phase change material emulsions and microencapsulated phase change material slurries: materials, heat transfer studies and applications. Renew Sustain Energy Rev. 2012;16(1):253–73. https://doi.org/10.1016/j.rser.2011.07.152
17. Cui Y, Xie J, Liu J, Pan S. Review of phase change materials integrated in building walls for energy saving. Procedia Eng. 2015;121:763–70. https://doi.org/10.1016/j.proeng.2015.09.027
18. Son HW, Heu CS, Lee HS, Kim SH, Mok JY, Kang S-W, et al. Enhanced thermal performance of lithium nitrate phase change material by porous copper oxide nanowires integrated on folded meshes for high temperature heat storage. Chem Eng J. 2020;391(2019):123613. https://doi.org/10.1016/j.cej.2019.123613
19. Xu G, Leng G, Yang C, Qin Y, Wu Y, Chen H, et al. Sodium nitrate – diatomite composite materials for thermal energy storage. Sol Energy. 2017;146:494–502. https://doi.org/10.1016/j.solener.2017.03.003
20. Gil A, Medrano M, Martorell I, Dolado P, Zalba B, Caeza LF. State of the art on high temperature thermal energy storage for power generation. Part 1—Concepts, materials and modellization. Renew Sustain Energy Rev. 2010;14(1):31–55. https://doi.org/10.1016/j.rser.2009.07.035
21. Zambotti A, Valentini F, Lodi E, Pegoretti A, Tyrpekl V, Kohutekova S, et al. Thermochemical heat storage performances of magnesium sulphate confined in polymer-derived SiOC aerogels. J Alloys Compd. 2021;895:162592. https://doi.org/10.1016/j.jallcom.2021.162592
22. >Fukushima M, Colombo P. Silicon carbide-based foams from direct blowing of polycarbosilane. J Eur Ceram Soc. 2012;32(2):503–10. https://doi.org/10.1016/j.jeurceramsoc.2011.09.009
23. Jana P, Santoliquido O, Ortona A, Colombo P, Sorarù GD. Polymer-derived SiCN cellular structures from replica of 3D printed lattices. J Am Ceram Soc. 2018;101(7):2732–8. https://doi.org/10.1111/jace.15533
24. Colombo P. Engineering porosity in polymer-derived ceramics. J Eur Ceram Soc. 2008;28(7):1389–95. https://doi.org/10.1016/j.jeurceramsoc.2007.12.002
25. Colombo P. Conventional and novel processing methods for cellular ceramics. Philos Trans R Soc A Math Phys Eng Sci. 2006;364(1838):109–24. https://doi.org/10.1098/rsta.2005.1683
26. Jana P, Zera E, Sorarù GD. Processing of preceramic polymer to low density silicon carbide foam. Mater Des. 2017;116:278–86. https://doi.org/10.1016/j.matdes.2016.12.010
27. Vallachira Warriam Sasikumar P, Zera E, Graczyk-Zajac M, Riedel R, Soraru GD, Dunn B. Structural design of polymer-derived SiOC ceramic aerogels for high-rate Li ion storage applications. J Am Ceram Soc. 2016;99(9):2977–83. https://doi.org/10.1111/jace.14323
28. Sorarù GD, Dalcanale F, Campostrini R, Gaston A, Blum Y, Carturan S, et al. Novel polysiloxane and polycarbosilane aerogels via hydrosilylation of preceramic polymers. J Mater Chem. 2012;22(16):7676–80. https://doi.org/10.1039/c2jm00020b
29. Colombo P, Mera G, Riedel R, Sorarù GD. Polymer-derived ceramics: 40 years of research and innovation in advanced ceramics. J Am Ceram Soc. 2010;93(7):1805–37. https://doi.org/10.1111/j.1551-2916.2010.03876.x
30. Bernardo E, Fiocco L, Parcianello G, Storti E, Colombo P. Advanced ceramics from preceramic polymers modified at

the nano-scale: a review. Materials (Basel). 2014;7(3):1927–56. https://doi.org/10.3390/ma7031927
31. Zambotti A, Valentini F, Lodi E, Pegoretti A, Tyrpekl V, Kohutekova S, et al. Thermochemical heat storage performances of magnesium sulphate confined in polymer-derived SiOC aerogels. J Alloys Compd. 2022;895:162592. https://doi.org/10.1016/j.jallcom.2021.162592
32. Zera E, Campostrini R, Aravind PR, Blum Y, Sorarù GD. Novel SiC/C aerogels through pyrolysis of polycarbosilane precursors. Adv Eng Mater. 2014;16(6):814–9. https://doi.org/10.1002/adem.201400134
33. Zambotti A, Biesuz M, Campostrini R, Carturan SM, Speranza SM, Ceccato R, et al. Synthesis and thermal evolution of polysilazane-derived SiCN(O) aerogels with variable C content stable at 1600°C. Ceram Int. 2020;47(6):8035–43. https://doi.org/10.1016/j.ceramint.2020.11.157
34. Barrett EP, Joyner LG, Halenda PP. The determination of pore volume and area distributions in porous substances. I. Computations from nitrogen isotherms. J Am Chem Soc. 1951;73(1):373–80. https://doi.org/10.1021/ja01145a126
35. Sing KSW. Reporting physisorption data for gas/solid systems with special reference to the determination of surface area and porosity. Pure Appl Chem. 1985;57(4):603–19. https://doi.org/10.1351/pac198557040603
36. Rouquerol J, Avnir D, Fairbridge CW, Everett DH, Haynes JM, Pernicone N, et al. Recommendations for the characterization of porous solids (Technical Report). Pure Appl Chem. 1994;66(8):1739–58. https://doi.org/10.1351/pac199466081739
37. Ruys AJ, Crouch IG. Siliconized silicon carbide. Met Ceram. 2021:211–83. https://doi.org/10.1016/B978-0-08-102869-8.00007-0
38. Stabler C, Reitz A, Stein P, Albert B, Riedel R, Ionescu E. Thermal properties of SiOC glasses and glass ceramics at elevated temperatures. Materials (Basel). 2018;11(2):1–18. https://doi.org/10.3390/ma11020279
39. Bhattarai B, Pandey A, Drabold DA. Evolution of amorphous carbon across densities: an inferential study. Carbon (NY). 2018;131:168–74. https://doi.org/10.1016/j.carbon.2018.01.103
40. Sorarù GD, Kundanati L, Santhosh B, Pugno N. Influence of free carbon on the Young's modulus and hardness of polymer-derived silicon oxycarbide glasses. J Am Ceram Soc. 2019;102(3):907–13. https://doi.org/10.1111/jace.16131
41. Biesuz M, Valentini F, Bortolotti M, Zambotti A, Cestari F, Bruni A, et al. Biogenic architectures for green, cheap, and efficient thermal energy storage and management. Renew Energy. 2021;178:96–107. https://doi.org/10.1016/j.renene.2021.06.068
42. Feng L, Dong S, Zhou H, Yang L, Yuan F, Yang Y, et al. n-Dodecanol nanocapsules with supramolecular lock shell layer for thermal energy storage. Chem Eng J. 2020;389(2019):124483. https://doi.org/10.1016/j.cej.2020.124483
43. Shameli K, Ahmad M Bin, Jazayeri SD, Sedaghat S, Shabanzadeh P, Jahangirian H, et al. Synthesis and characterization of polyethylene glycol mediated silver nanoparticles by the green method. Int J Mol Sci. 2012;13(6):6639–50. https://doi.org/10.3390/ijms13066639
44. Nguyen VL, Laidani NB, Sorarù GD. N-doped polymer-derived Si(N)OC: the role of the N-containing precursor. J Mater Res. 2015;30(6):770–81. https://doi.org/10.1557/jmr.2015.44
45. Fredi G, Dirè S, Callone E, Ceccato R, Mondadori F, Pegoretti A. Docosane-organosilicamicrocapsules for structural composites with thermal energy storage/release capability. Materials (Basel). 2019;12(8):1286. https://doi.org/10.3390/ma12081286
46. Valentini F, Dorigato A, Pegoretti A, Tomasi M, Sorarù GD, Biesuz M. Si_3N_4 nanofelts/paraffin composites as novel thermal energy storage architecture. J Mater Sci. 2021;56(2):1537–50. https://doi.org/10.1007/s10853-020-05247-5
47. Feng L, Song P, Yan S, Wang H, Wang J. The shape-stabilized phase change materials composed of polyethylene glycol and graphitic carbon nitride matrices. Thermochim Acta. 2015;612:19–24. https://doi.org/10.1016/j.tca.2015.05.001
48. Zambotti A, Caldesi E, Pellizzari M, Valentini F,Pegoretti A, Dorigato A, et al. Polymer-derived silicon nitride aerogels as shape stabilizers for low and high-temperature thermal energy storage. J Eur Ceram Soc. 2021;41(11):5484–94. https://doi.org/10.1016/j.jeurceramsoc.2021.04.056

How to cite this article: Zambotti A, Biesuz M, Bortolotti M, Dorigato A, Valentini F, Fredi G, et al. Low-temperature thermal energy storage with polymer-derived ceramic aerogels. Int J Appl Ceram Technol. 2023;20:39–50. https://doi.org/10.1111/ijac.14158